Reduction in CD11c$^+$ microglia promotes secondary progression in autoimmune demyelination

Olga V. Chechneva[1,2*], Florian Mayrhofer[2], Zhanna Dariychuk[2], Anthony Zhen[2], Daniel J. Daugherty[1,2], Peter Bannerman[2], Angela M. Hanson[2], David Pleasure[2], Athena Soulika[2], Wenbin Deng[1,2*]

[1]Department of Biochemistry and Molecular Medicine, UC Davis, Sacramento, CA 95817; [2]IPRM, Shriners Hospital for Children, Sacramento, CA 95817

Corresponding authors:

Olga V. Chechneva

Department of Biochemistry and Molecular Medicine

School of Medicine, UC Davis

2425 Stockton Blvd, Sacramento, CA, 96817

Phone: 916-453-2250

Fax: 916-453-2288

Email: ochechneva@ucdavis.edu

Wenbin Deng

Department of Biochemistry and Molecular Medicine

School of Medicine, UC Davis

2425 Stockton Blvd, Sacramento, CA, 96817

Phone: 916-453-2287

Fax: 916-453-2288

Email: wbdeng@ucdavis.edu

Running title: CD11c$^+$ microglia in secondary progressive EAE

Conflict of interest: The authors have declared that no conflict of interest exists.

Abstract

Secondary progressive multiple sclerosis (SPMS) is a common outcome of relapsing-remitting form of multiple sclerosis (MS). The cellular and molecular mechanisms of SPMS remain unclear and there is an unmet need for treatments to prevent or stop secondary progression (SP). Here we demonstrate that reduction in CD11c$^+$ microglia promotes disperse coalescent immune cell infiltration of the spinal cord white matter causing clinical deterioration and SP in experimental autoimmune encephalomyelitis (EAE), an animal model of MS. Knockout of *p38a* in CD11c$^+$ cells in female mice resulted in reduction in CD11c$^+$ microglia number and high incidence of SP EAE associated with immune cell parenchymal infiltration. In contrast, increased numbers of CD11c$^+$ microglia in males resulted in detention of immune cells in perivascular areas and prevented SP. We conclude that CD11c$^+$ microglia are essential to halt immune cells from re-entering CNS parenchyma in SP EAE. Our data uncovered a sex-biased mechanism of p38α signaling in CD11c$^+$ microglia and revealed a novel regulatory function of CD11c$^+$ microglia in chronic autoimmune neuroinflammation.

Introduction

Multiple sclerosis (MS) is an autoimmune demyelinating disorder characterized by chronic inflammation, myelin loss and axonal degeneration. MS displays a dynamic clinical phenotype with the most common appearance as a relapsing-remitting form (RRMS). Within a decade of the first diagnosis, 30% of RRMS patients with, and 50% without disease modifying therapies develop secondary progression (SP) of clinical deficits (1, 2). Secondary progressive MS (SPMS) is associated with poor clinical prognosis (3). Male sex, older age at onset and high early relapse frequency are the risk factors for developing SPMS (4). There are no proven therapies to stop or prevent SPMS. Defining the cellular and molecular mechanisms underlying SPMS is needed for finding effective therapies.

$CD11c^+$ cells play an active role in the pathogenesis of MS. $CD11c^+$ classical dendritic cells (cDC) are professional antigen-presenting cells that process immunogenic epitopes of different size antigens through a major histocompatibility complex class II and induce proliferation and polarization of naïve and effector T cells (5, 6). Meningeal and perivascular cDC are responsible for the reactivation of myelin-primed T cells, permitting the progression of paralysis in experimental autoimmune encephalomyelitis (EAE), an animal model of MS (5-7). $CD11c^+$ monocyte-derived DC (moDC) emerge from circulating $CD11b^+Ly6C^{hi}$ monocytes infiltrating the CNS before the onset of EAE clinical symptoms, where they induce demyelination through release of iNOS-generated reactive oxygen species (8, 9). The majority of these cells undergo transcriptional reprograming toward an Arginase-1 expressing neuroprotective phenotype before EAE remission (9). moDCs are unable to present antigen and induce T cell proliferation and polarization, but exert efficient phagocytic activity (5, 9).

$CD11c^+$ microglia are present in the CNS parenchyma under steady-state condition and found in close proximity to astrocyte end-feet (10-12). $CD11c^+$ microglia have poor antigen presenting

capacity (5, 7, 13, 14). Increase in CD11c$^+$ microglia precedes the onset of EAE clinical symptoms (15, 16) and a growing number of evidence indicates that CD11c$^+$ microglia possess a neuroprotective function in disease. Increase in CD11c$^+$ microglia was associated with a reduction of EAE clinical disability (17), alleviation of cuprizone-induced demyelination (18), as well as decrease in amyloid plaque numbers and cognitive improvement in a transgenic model of Alzheimer's disease (19). Increase in CD11c$^+$ microglia is dependent on colony-stimulating factor 1 receptor (CSF1R) and its ligands CSF1 and IL-34 and can also be induced by ablation of signal regulatory protein-α or its ligand CD47 (18). The role of CD11c$^+$ cells in SP remains poorly defined.

Among the signaling pathways activated in chronic autoimmune inflammation is mitogen-activated protein kinase 14 (p38*a*), a member of the p38 MAPK family (20). Expression of p38α is upregulated in active and chronic lesions in patients with MS (21). cDC depend on p38α signaling to promote differentiation of uncommitted T cells toward T_H17 phenotype in MS and EAE (22, 23). Knockout of *p38a* in CD11c$^+$ cells results in mild EAE phenotype (22, 24). A sex-dependent role of p38α in EAE has been reported in myeloid cells, where pharmacological inhibition or myeloid cell knockout of p38α ameliorated EAE clinical symptoms and inflammation in female mice (24). However, the role of p38α in SP remains unknown.

Here we report that reduction in CD11c$^+$ microglia results in disperse coalescent CNS infiltration and transition from mild EAE phenotype to exacerbation of EAE clinical symptoms around 30 days post immunization (dpi), that we defined as SP EAE. We found that knockout of *p38a* in CD11c$^+$ cells (*KO*) reduced proliferation of CD11c$^+$ microglia under immune stimulation in females. *KO* females display lower numbers of CD11c$^+$ microglia in EAE and high incidence of SP EAE, triggered by immune infiltration. In contrast, increased numbers of CD11c$^+$ microglia in *KO* males resulted in clustering of immune cells in perivascular areas and harnessing clinical transition to SP EAE. Together, our data identified a sex-dependent role of p38α in CD11c$^+$ microglia and demonstrate a

novel neuroprotective function of CD11c$^+$ microglia as a critical regulator of CNS immune cell infiltration and SP EAE.

Results

Reduction in CD11c$^+$ microglia and disperse parenchymal infiltration are distinctive features of SP EAE

EAE in C57BL/6 wild type (WT) mice induced with MOG_{35-55} emulsion prepared by sonication results in severe phenotype with chronic paralysis (score 3.5 – 4.5) throughout the disease course (25). We found that EAE induction using MOG_{35-55} emulsion prepared by syringe homogenization rather than sonication results in three clinical phenotypes: mild non-progressive (NP) (42%), severe (31%) and initially mild with SP around 30 dpi (27%) (Fig. 1A). Mild NP EAE was defined by mild clinical phenotype with abnormal gait/paresis (maximum score 3) throughout EAE course. Severe EAE displayed chronic paralysis (score 3.5 – 4.5) throughout the disease course. SP was identified by transition from mild to severe EAE around 30 dpi with an increase in clinical score by 1-2.5 points. SP EAE constituted ~40% of mice with initially mild EAE.

To define pathological features of SP EAE, we compared infiltration at EAE peak, chronic mild NP, severe and SP EAE. Histological analysis revealed a distinctive disperse coalescent infiltration of the spinal cord white matter in SP mice compared to EAE peak, where infiltrates were compact and formed disconnected patches (Fig. 1B). Diffuse scattering of immune cells in the parenchyma with lesser density than SP was observed in severe EAE. In mild NP EAE, immune cells were concentrated at the perivascular areas (Fig. 1B). We characterized immune cell infiltrates in the CNS using flow cytometry. Increase in T_H1 and T_H17 effector cells was evident in SP compared to mild NP and severe EAE, supporting the role of both, T_H17 and T_H1 cells, in SPMS (26-28) (Supplementary Fig. 1A-D). At EAE peak, the number of CD45$^+$ cells (Fig. 1C, H), including neutrophils (Fig. 1D, I) and macrophages/monocytes (Fig. 1E, J) was increased compared to mild NP, severe and SP. However,

at SP, the number of neutrophils and macrophages/monocytes was significantly higher compared to mild NP and severe EAE (Fig. 1C-E, H-J). We found no differences in numbers of $CD11b^{+}CD45^{lo}$ microglia between EAE groups (Fig. 1E, K).

The number of $CD11c^{+}$ cells was increased at EAE peak and SP compared to mild NP and severe EAE (Fig. 1F, L). However, EAE peak showed significantly higher number of $CD11c^{+}$ cells compared to SP. We differentiated $CD11c^{+}$ cells in three populations by expression of CD45 and CD11b: 1) $CD11c^{+}CD11b^{-}CD45^{hi}$ or cDC, 2) $CD11c^{+}CD11b^{+}CD45^{hi}$ or moDC, and 3) $CD11c^{+}CD11b^{+}CD45^{lo}$ or $CD11c^{+}$ microglia (Fig. 1G). To define population of $CD11c^{+}$ microglia by FACS, we found gating on $CD11b^{+}$ and $CD45^{+}$ cells from the pool of $CD11c^{+}$ cells to be more accurate due to the lack of clear separation of macrophages/monocytes from microglia within $CD11b^{+}CD45^{int}$ population. cDC (Fig. 1G, M) and moDC (Fig. 1G, N) were elevated at EAE peak and SP compared to mild NP and severe EAE. Notable, while increase in $CD11c^{+}$ microglia was evident at EAE peak, mild NP and severe EAE, SP mice showed significant reduction in $CD11c^{+}$ microglia population (Fig. 1G, O). Gating on $CD11c^{+}$ microglia from the pool of $CD11b^{+}CD45^{lo}$ microglia resulted in similar outcome (Supplementary Fig. 1E-F). The proportion of $CD11c^{+}$ microglia among $CD11c^{+}$ cells was reduced at EAE peak and SP (Supplementary Fig. 1G). No sex-dependent differences in immune cell populations were found in all experimental conditions. We conclude that reduction in $CD11c^{+}$ microglia and disperse parenchymal infiltration contribute to the mechanism of SP EAE.

Knockout of *p38α* in $CD11c^{+}$ cells promotes parenchymal infiltration and SP EAE in female mice

p38α MAPK controls the function of $CD11c^{+}$ cells in EAE and MS (22-24). To determine the role of p38α MAPK in $CD11c^{+}$ cells in SP EAE, we followed EAE clinical symptoms in $p38\alpha^{\Delta CD11c}$ (*KO*) and $p38\alpha^{fl/fl}$ control (*Floxed*) mice for 60 days. As previously reported (22, 24), *KO* mice initially

displayed mild EAE clinical symptoms compared to *Floxed* cohorts, that developed severe EAE following induction with MOG_{35-55} emulsion prepared by sonication (Fig. 2A, Table 1). No sex differences were evident at the initial course of disease in *Floxed* mice, however *KO* females showed delay in EAE onset and peak compared to *KO* males (Fig. 2A, Table 1). Notably, around 30 dpi, 58% of *KO* females developed SP (Fig. 2A, Table 1). No SP of EAE clinical symptoms was observed in *KO* males (Fig. 2A, Table 1). As indicator for efficient *p38α* knockout, low expression level of the activated form of p38 MAPK, phospho-p38 MAPK, was found in $CD11c^+$ splenocytes in *KO* mice after LPS stimulation, with no sex difference (Supplementary Fig. 2A-B). We conclude that in female mice p38*α* signaling in $CD11c^+$ cells controls SP EAE.

To evaluate the mechanism of SP in *KO* females, we examined EAE pathology in the lumbar spinal cord of *KO* and *Floxed* female and male mice using LFB & Cresyl Violet staining. In *Floxed* mice we found infiltration and demyelination with no sex difference (Fig. 2B-C). In the spinal cords of *KO* males and females we identified sex-specific phenotypes. *KO* males displayed clusters of immune cells accumulated at the perivascular areas and meninges (Fig. 2B-C). In contrast, *KO* SP females showed disperse infiltration of immune cells and demyelination throughout white matter. *KO* NP females showed minimal immune cell parenchymal and perivascular presence with no distinguishable demyelination (Fig. 2B-C).

Infiltrating myelin-specific T cells and myeloid cells cause demyelination and clinical progression in EAE and MS (29-32). In *KO* SP females, $CD4^+$ cells, were found within white matter parenchyma (Fig. 2D). In *KO* males, $CD4^+$ cells clustered at perivascular sites with rare parenchymal presence (Fig. 2E). The number of parenchymal $CD4^+$ T cells in the lumbar spinal cord of *KO* SP females was significantly increased compared to *KO* males (Fig. 2F). Flow cytometry analysis of immune cells isolated from the brain and spinal cord at 30 dpi showed increase in $CD3^+$ T cells in *KO* SP females (Fig. 2G). T_H17 cells are dependent on p38α signaling in cDC (22). We found that INF-γ^+ T_H1 cells

dominated in numbers (Fig. 2H) and were efficient to induce SP in *KO* females. No significant differences in IL-17$^+$ T cells were found between *KO* SP females and *KO* males (Fig. 2H).

Assessing myeloid cell infiltration, we found Iba1$^+$ or lectin$^+$ macrophages/monocytes or reactive microglia scattered throughout white matter parenchyma in *KO* SP females (Fig. 3A, C, E). In males, macrophages/monocytes were clustered along perivascular spaces and meninges (Fig. 3B, D, F). Expression of CD45 confirmed reduced parenchymal infiltration in *KO* males compared to *KO* SP females (Fig. 3E-F). In males, ramified or partially activated Iba1$^+$ microglia were morphologically distinguishable from infiltrating macrophages/monocytes present at the meninges (Fig. 3F). In females, microglia could not be differentiated from macrophages/monocytes by morphology (Fig. 3E). We used FACS to further quantify immune cells. The total number of CD45$^+$ cells was significantly increased in the brain and spinal cord of *KO* SP females (Fig. 3G, J). We found increase in Ly6G$^+$ neutrophils (Fig. 3H, K) and CD11b$^+$CD45^{hi} macrophages/monocytes (Fig. 3I, L). There were no differences in the numbers of CD11b$^+$CD45^{lo} microglia between groups (Fig. 3I, M). We conclude that parenchymal invasion of T cells, neutrophils and macrophages/monocytes drives SP EAE in *KO* females.

Knockout of *p38α* results in reduction in CD11c$^+$ microglia in *KO* females in EAE

To evaluate the mechanism of SP in *KO* females, we examined CD11c$^+$ cells. We used expression of eGFP under the CD11c promoter, to track CD11c$^+$ cells, as commercially available anti-CD11c antibodies were not able to detect CD11c$^+$ cells in PFA perfused tissues (11, 33). In *KO* SP females, the majority of eGFP$^+$ cells found in the white matter parenchyma were moDC co-expressing CD11b (Fig. 4A). In *KO* males, eGFP$^+$ microglia were distinguishable by morphology (Fig. 4B, arrows). We also identified DC-like CD11c$^+$ microglia with stellate thick processes within spinal cord white matter in *KO* males (Fig. 4B, arrowhead). The absolute number of CD11c$^+$ cells isolated from the brain and spinal cord was significantly higher in *KO* SP females (Fig. 4C-D). There were no

differences in the numbers of cDC between groups (Fig. 4F). moDC were significantly increased in *KO* SP females compared to all other groups (Fig. 4G). Both, *KO* NP and SP females had significantly lower numbers of $CD11c^+$ microglia compared to *Floxed* mice and *KO* males (Fig. 4H). Gating on $CD11c^+$ microglia from the pool of $CD11b^+CD45^{lo}$ microglia resulted in the similar outcome (Supplementary Fig. 3A-B). We conclude that in female mice p38α signaling controls $CD11c^+$ microglia number.

Cell renewal is required for maintaining the cell population. We questioned whether reduction in $CD11c^+$ microglia in *KO* females was due to altered self-renewal. We examined the rate of $CD11c^+$ cell proliferation using EdU labeling and flow cytometry. Healthy mice showed no differences in $CD11c^+$ microglia numbers and proliferation rate between *Floxed* and *KO* groups of both sexes (Supplementary Fig. 4A-B). MOG-immunized mice that did not develop clinical symptoms in response to immune stimulation, display a higher number of CNS associated $CD45^+$ cells at 30 dpi compared to healthy mice (Supplementary Fig. 4C). We examined the rate of $CD11c^+$ cell proliferation under this condition (Supplementary Fig. 4D). No differences in the number and proliferation rate of cDC were found between *Floxed* and *KO* mice of both sexes (Supplementary Fig. 4E-F). The number of moDC was significantly increased in *KO* males compared to *KO* females and *Floxed* mice, however there was no difference in their proliferation rate (Supplementary Fig. 4G-H). *KO* females showed significant reduction in the number and the proliferation rate of $CD11c^+$ microglia compared to *KO* males (Supplementary Fig. 4I-J). Proliferation rate of macrophages/monocytes and total microglia were not different between experimental groups (Supplementary Fig. 4K-M). We conclude that p38α signaling controls $CD11c^+$ microglia proliferation during immune response. Together, reduction in $CD11c^+$ microglia in *KO* females promotes disperse coalescent parenchymal infiltration and SP EAE.

Discussion

Like MS, EAE is a complex pathological condition, characterized by high variability of clinical symptoms. EAE variability creates the opportunity to model a variety of clinical mechanisms featured in MS. Importantly, there is a lack of models for SPMS.

Our previously described EAE model of MOG_{35-55} prepared by sonication consistently causes severe EAE in WT mice (25). Changes in MOG epitope and/or Mycobacterium tuberculosis biochemical composition by sonication may explain an enhanced immune response to immunization in this model (34). We newly found that syringe emulsification of MOG_{35-55}, results in three distinct EAE phenotypes in WT mice: mild NP, severe and SP EAE. In our model, SP occurs in ~40% of mice that initially develop mild disease and spontaneously progress to severe form with deterioration of clinical symptoms around 30 dpi. A similar course of disease has been reported in non-obese diabetic mice that develop SP around 30 dpi after MOG_{35-55} immunization (35-37). However, non-obese diabetic mice gradually develop hyperglycemia at 12-15 weeks of age that alters the cellular and molecular mechanism of SP EAE (38). Therefore, our model adds to a limited number of valuable tools to study the mechanism of SP EAE and develop treatments for SPMS.

Using our model, we made important finding that in mild EAE a reduction in the numbers of $CD11c^+$ microglia contributes to disperse coalescent parenchymal infiltration and SP EAE. In contrast, high numbers of $CD11c^+$ microglia and immune cells restrained to perivascular spaces were found in animals with mild EAE that did not develop progression. Our data indicate that $CD11c^+$ microglia play a critical role in controlling CNS parenchymal infiltration in SP EAE. We support our finding in mice lacking p38α MAPK in $CD11c^+$ cells which initially develop mild EAE and showed that high incident of SP EAE in female *KO* mice was associated with the reduction in $CD11c^+$ microglia and disperse parenchymal infiltration. Our findings are in line with a recent study, where depletion of microglia with antagonist of CSF1R, PLX3397, resulted in expansion of $CD4^+$ T cells and

exacerbation of SP EAE in non-obese diabetic mice (35). This study, however, did not differentiate the role of CD11c$^+$ microglia from other microglia subtypes.

The mechanism how CD11c$^+$ microglia controls CNS infiltration remains unclear. In the white matter of *KO* males, where infiltration was prevented, we could identify two morphologically distinct CD11c$^+$ microglia populations: DC-like microglia and microglia with partially activated phenotype. The presence of DC-like CD11c$^+$ microglia in close proximity to glia limitans was reported in the brain, spinal cord and optic nerve parenchyma of healthy mice, suggesting their role in astrocyte glia limitans organization (11). We found that immune cell parenchymal infiltration in *KO* females was associated with the presence of hypertrophic reactive astrocytes strongly expressing CCL2 (Supplementary Fig. 5A-C). In contrast, high number of CD11c$^+$ microglia and restricted immune cell infiltration were correlated with moderate CCL2 expression. A similar pathological phenotype of restricted immune infiltration was found in EAE mice with CNS specific CCL2 knockout (31) and limited T cell entry was reported in EAE mice with astrocyte specific CCL2 deletion (39). CCL2 has been identified as a positive regulator of CD11c$^+$ microglia population in the healthy CNS (17). Our data suggest that there is a CCL2 dose-dependent astrocyte - CD11c$^+$ microglia cross talk regulating CNS infiltration in SP EAE. Detailed characterization of CD11c$^+$ microglia will help to understand their full function in SP EAE and other neuroinflammatory disorders.

We found that in female mice, proliferation of CD11c$^+$ microglia after immune stimulation was dependent on p38α signaling. It has been previously reported that hormone-dependent sexual dimorphism of the immune response is regulated by p38 MAPK signaling. In microglia, p38 MAPK signaling was identified as a cause of neuropathic and inflammatory pain in males but not females in animal models of chronic constriction injury and mechanical allodynia (40, 41). Testosterone-dependent increase in p38 MAPK phosphorylation in splenic and peritoneal macrophages was reported in male mice after trauma-hemorrhage (42). Knockout of p38α in CD11c$^+$ cells protects both, female and male mice, at the initial EAE phase (22, 24). However, delay in EAE peak in female

KO mice may indicate a sex-dependent function of p38α in cDC (Table 1) and explain the fraction of *KO* NP females with reduced parenchymal immune cell presence, possibly due to inefficient T-cell priming. moDC is another cell candidate that may contribute to p38α-dependent neuroprotection in *KO* NP females. Reduction of EAE clinical symptoms was found in female but not male mice with knockout of p38α in LyzM$^+$ myeloid cells, including moDC (24). Moreover, pharmacological inhibition of p38 MAPK signaling protected female mice at EAE acute phase (24). In contrast to cDC and moDC, our study highlights the beneficial role of p38α in maintaining CD11c$^+$ microglia population in female mice that is critical to preventing SP EAE. Together, the diverse functions of p38α signaling depending on the cell type and sex may explain the reason why many of p38 MAPK inhibitors failed to fulfill their expectations in clinical trials (43, 44).

Based on our data and published reports, here we diagram the cellular model of SP EAE (Fig. 5A). Following recovery from initial EAE phase, T cells are reactivated by cDC in the leptomeninges and perivascular spaces separated from CNS parenchyma by the basement membrane and glia limitans (5-7, 45). Reduction in CD11c$^+$ microglia (our observation) allows T cells to cross the basement membrane and glia limitans and enter CNS parenchyma. As suggested by Giles et al., T cells expand within CNS parenchyma (5), causing clinical onset of SP and increase in astrocyte derived CCL2 that attracts myeloid cells (30, 31, 39). Invading myeloid cells damage oligodendrocytes, myelin and axons, resulting in exacerbation of EAE clinical symptoms at SP (30-32, 46, 47). It remains to be determined whether increase in parenchymal T and myeloid cells at SP is due to increase in number of cells entering CNS or cells that entered parenchyma subsequently undergo the expansion.

Molecular triggers of SP EAE are still unclear. Secondary antigenic epitope spreading may cause clinical relapse and initiate SP EAE (48). However, it remains unknown why only a fraction of animals develop SP EAE. Other questions, such as why SP EAE follows a 30 days post immunization pattern and what is causing the drop in CD11c$^+$ microglia need to be addressed to understand molecular mechanism of SP EAE and SPMS.

Together, we showed that reduction in CD11c$^+$ microglia is critical to parenchymal infiltration and clinical deterioration in SP EAE. Our study concludes that helping to maintain CD11c$^+$ microglia or boosting their population are legitimate aims to develop therapies to stop or prevent SPMS. Further studies of CD11c$^+$ microglia and their function in EAE and MS are warranted to move this strategy forward.

Materials and Methods

Animals

Mice carrying the *p38α* floxed allele [B6.129-*Mapk14*<tm1.2Otsu.] were crossed with mice expressing Cre recombinase under the CD11c promoter (C57BL/6J-Tg(*Itgax*-cre-EGFP)4097Ach/J, JAX stock #007567). The offsprings were genotyped for the presence of *p38α* floxed allele and *Cre* insert as described earlier (49). Female and male $p38\alpha^{\Delta CD11c}$ and $p38\alpha^{fl/fl}$ mice were used for experiments. Female and male C57BL/6 mice 12 weeks old were used to study SP EAE in WT mice. Animals were maintained in accordance to the NIH Guide for the Care and Use of Laboratory Animals. Experimental protocols were approved by the Institutional Animal Care and Use Committee at the University of California, Davis.

EAE induction

EAE was induced in female and male mice at the age of 12 weeks as described earlier (25). In brief, mice were injected subcutaneously at two flank sites with an emulsion of MOG_{35-55} (New England Peptide) in incomplete Freund's adjuvant supplemented with 500 µg Mycobacterium tuberculosis H37Ra (Difco). EAE in $p38\alpha^{\Delta CD11c}$ mice was induced with MOG_{35-55} (300 µg) emulsion prepared by quick sonication (3x5 sec on ice). To model SP EAE in WT mice, MOG_{35-55} (150 µg) was homogenized in 2 syringes connected by a stopcock (twice 10 min with 3 h interval on ice). Emulsion was kept in the dark at 4^0C between mixing and before assembling into individual doses in syringes. Mice received 200 ng of pertussis toxin (PTX) (List Biological Labs) intraperitoneally (i. p.) on day 0 and 2. The severity of clinical symptoms was evaluated using a standard neurological scoring system for EAE: 0 - no deficit; 0.5 - mild loss of tail tone; 1 - complete loss of tail tone; 1.5 - mildly impaired righting reflex; 2 - abnormal gait (ataxia) and/or impaired righting reflex; 2.5- single hind limb paresis and ataxia; 3 - double hind limb paresis; 3.5 - single limb paralysis and paresis of second limb / paresis of both hind limbs and weakness of front limbs; 4 - full paralysis of two limbs; 4.5 -

hind limb paralysis with hind body paresis; 5 – moribund or death. Animals were monitored and scored daily.

Histology and pathological scoring

Histological analysis was performed as described earlier (25). Briefly, mice were anesthetized with isoflurane and perfused with ice cold phosphate buffered saline (PBS). Lumbar spinal cords were dissected, cryopreserved in 20% sucrose, embedded in OCT compound and cut in 15 µm sections on the cryostat. For Luxol Fast Blue (LFB) staining, sections were incubated with 0.1% LFB solution at 60^0C for 16 h followed by differentiation with 0.05% lithium carbonate and co-stained with 0.1% Cresyl Violet. For Hematoxylin & Eosin (H&E) staining, sections were stained with Mayer's hematoxylin followed by 1% eosin. Slides were mounted using Cytoseal-60 medium and images were acquired on Keyence BZ-9000 microscope. For pathological assessment, for each animal, six sections of the lumbar spinal cord in the interval of 180 µm were scored by blinded investigator for infiltration, vacuolation caused by swollen axon sheaths and demyelination. We used following scoring system: 0 - absence of lesion and infiltration; 1 - not clearly visible lesions and infiltration, 2 – clearly visible lesions and infiltration, 3 – prominent multifocal lesions and infiltration, 4 – marked continuous lesions and infiltration (50).

Immunohistochemistry

For immunostaining, sections were washed with PBS to remove residues of OCT compound. Nonspecific binding of antibodies was blocked using 10% normal serum in 0.2% Triton-X in PBS. Samples were incubated with rabbit anti-Iba1 (ionized calcium binding adaptor molecule 1; 1:500; Wako 019-19741), rabbit anti-CD4 (1:200; Abcam ab183685), rat anti-CD45 (1:200; SouthernBiotec 1660-01), FITC conjugated lectin from Lens culinaris (1:300; Sigma), chicken anti-GFP (1:500, Abcam ab13970), rat anti-CD11b (1:100, BD Pharmingen 550282), rabbit anti-CCL2 (1:200, Millipore AB1834P) overnight at 4 °C. Fluorophore-conjugated secondary antibodies Alexa Fluor

488, 555 or 647 (1:1000; Life Technologies) were used to detect primary antibody. Slides were mounted using DAPI Fluoromount-G (SouthernBiotech). Images were acquired on Nikon Eclipse TE 2000-E microscope using a D-Eclipse C1si camera (Nikon). For DAB staining, sections were treated with 1% H_2O_2 to stop endogenous peroxidase activity before incubation with blocking serum. After primary antibodies, sections were incubated with HRP-conjugated secondary antibody. Positive signal was visualized using ImmPACT DAB Peroxidase substrate kit (Vector labs). Images were acquired on Olympus BX61-DSU microscope using Hamamatsu ORCA-ER camera (Hamamatsu Photonics). For fluorescent and DAB staining negative controls omitting primary antibody were performed. Images were processed using Adobe Photoshop CC.

FACS analysis

Mice were deeply anesthetized and transcardially perfused with ice-cold PBS for 3 min with a flow rate at 3 ml/min. Brains and spinal cords were dissected and placed in ice-cold HBSS (Hank's Balanced Salt Solution) in 2.5 cm culture dish. For tissue digestion, papain resulted in a higher cell yield compared to collagenase. However, we found that papain digestion resulted in the loss of CD11c expression on the cell surface. Therefore, CNS tissue for all FACS experiments were digested using collagenase. Collagenase D (Roche) 1 mg/ml and 0.02 mg/ml with 100 U/ml DNAse I (Worthington) were added to each dish (final concentration), tissue was chopped into ~1-2 mm^3 pieces and incubated while shaking at 100 rpm at 37 °C with 5% CO_2 for 20 min. Enzymatic activity was blocked by EDTA at final concentration 2 mM. On ice, tissue was homogenized in Dounce homogenizer (5-8 strokes) and cell suspension was passed through a 100 µm cell strainer (Corning) in 50 ml falcon tubes. Cells were collected at 350 x g for 5 min at 4°C. To remove myelin and dead cells, cell pellet was resuspended in 37% Percoll (GE Healthcare). Cells were transferred to 15 ml falcon tube and centrifuged at 500 x g for 15 min with 0 brake at 4^0C. Myelin layer was aspirated and cell pellet was resuspended in cold 0.5 ml RBC lysis buffer (Biolegend, 420301), transferred and

incubated in 15 ml falcon tubes for 30 sec on ice. 5 ml PBS was added to each tube after incubation and cells were separated by centrifugation at 350 x g at 4^0C for 5 min. Cells were resuspended in FACS buffer (PBS plus 1% BSA and 0.1% sodium azide), counted using hemocytometer and transferred to staining plates (Fisher Scientific, 12565502). After 15 min blocking of Fc receptors with CD16/CD32 antibody (BD Pharmingen) on ice, cells were stained with fluorophore-conjugated antibodies: CD11b BV605 (1:200, clone M1/70, Biolegend), CD45 PerCP-Cy5.5 (1:200, clone 30-F11, Biolegend), Ly6G APC-Cy7 (1:200, clone 1A8, BD Biosciences), CD11c FITC (1:100, clone N418, Biolegend), CD11c APC (1:100, clone N418, Biolegend) on ice for 30-60 min. Cells were washed twice with FACS buffer and once with PBS to remove residues of BSA, then incubated with dead cell dye, Zombie red (1:1000 in PBS, Biolegend) for 15 min on ice. After washing, cells were analyzed on Attune NxT Acoustic Focusing Cytometer (Life Technologies). For cytokine detection, cells were counted and incubated in RPMI-1640 medium supplemented with 10% FBS, 2 mM glutamax, 1 mM sodium pyruvate, 0.1 mM NEAA, 100 U penicillin/streptomycin, 50 µM β-ME with Golgi plug (BD Biosciences, 555029) for 1 h at 37^0C with 5% CO_2. Phorbol 12-myristate 13-acetate (PMA, 50 ng/ml final concentration) and ionomycin (750 ng/ml final concentration) were added to incubate for 4-5 h. Fc receptors were blocked as described above and cells were stained with CD3e FITC (1:200, clone 145-2C11, BD Pharmingen) or CD3e PE-Cy7 (1:200, clone 145-2C11, BD Pharmingen). Dead cells were labeled using Violet fluorescence reactive dye for 20 min on ice (1:1000, ThermoFisher, Cat# L34963). Cells were fixed for 15 min on ice using BD Cytofix/Cytoperm reagent (BD Biosciences, 554722). After washing with BD Perm/Wash (BD Biosciences, 554723) twice, cells were incubated overnight with IFN-γ APC (1:25, Clone XMG1.2, Biolegends) and IL-17 PE (1:50, Clone TC11-18H10, BD Pharmingen) in Perm/Wash buffer. After washing with FACS buffer, cells were analyzed on Attune NxT Acoustic Focusing Cytometer (Life Technologies). Unstained cells, single stain controls and stained AbC Total Antibody Compensation beads (Thermo Fisher, A10497) were used for each experiment to determine compensation

parameters. For isotype control of fluorescence minus one, the specific antibody was substituted by fluorophore-conjugated isotype control. Acquired data were analyzed using FlowJo software (TreeStar). The absolute number of specific cell type was determined by multiplying the total number of live cells isolated from the CNS to the proportion of specific cell type acquired by flow cytometer. The quantitative data were presented in absolute numbers.

EdU labeling and analysis

EdU is a thymidine nucleoside analog that incorporates into DNA during S-phase of the cell cycle. To label proliferating cells, animals were pulsed with 12 mg/kg EdU i.p. twice with 12 h interval. 24 h after the first injection, animals were deeply anesthetized and perfused with ice cold PBS. Brain and spinal cord were dissected, and cells were isolated as described above. Fc receptors were blocked with CD16/CD32 antibody (BD Pharmingen) for 15 min on ice and cells were stained with fluorophore-conjugated antibodies: CD11b BV605 (1:200, clone M1/70, Biolegend), CD45 PerCP-Cy5.5 (1:200, clone 30-F11, Biolegend) and CD11c APC (1:100, clone N418, Biolegend) for 30 min on ice. Zombie violet (1:1000, Biolegend) was used to label dead cells. Cells were then fixed with 4% PFA for 15 min at RT. After washing with 1% BSA in PBS, cells were permeabilized with saponin-based permeabilization and wash reagent (Invitrogen, Click-iT Plus EdU Kit) for 15 min at RT. Residues of permeabilization buffer were removed by centrifugation at 350 x g for 5 min. EdU was detected by incubation with freshly prepared Click-iT cocktail containing Tris-HCl (100 mM, pH 7.6), 2 mM $CuSO_4$, 2.5 µM Sulfo-Cy3 Azide (Limiprobe) and 100 mM ascorbic acid for 15 min at RT in the dark. Cells were washed with FACS buffer and analyzed on Attune NxT Acoustic Focusing Cytometer (Life Technologies). For Cy3 single stain compensation control we used cells isolated from the bone marrow. Proliferation rate was determined as a percentage of EdU^+ cells from the specific cell population.

p38 MAPK activity

p38 MAPK activity was assessed by quantifying phospho-p38 MAPK expression level. *KO* and *Floxed* female and male mice were intraperitoneally injected with 3 mg/kg LPS (O111:B4, Sigma). 24 h after, mice were deeply anesthetized and spleens were isolated, cut into smaller pieces in ice cold HBSS, and enzymatically digested for 20 min at 37^0C. Digested tissue was passed through a 70 µm cell strainer using the backside of 1 ml syringe into 50 ml falcon tubes. Cells were pelleted by centrifugation at 350 x g at 4^0C for 5 min and resuspended in ice cold 1 ml RBC lysis buffer. After washing and centrifugation, cells were resuspended in MACS buffer (PBS with 0.5% BSA and 2 mM EDTA) and counted using hematocytometer. After centrifugation, cells were resuspended and incubated in MACS buffer containing Fc blocker and CD11c MicroBeads (Miltenyi Biotec) according to manufacturer instruction. $CD11c^+$ cells were isolated using LS columns (Miltenyi Biotec, Cat# 130-108-338), pelleted and processed for staining. After Fc receptor blocking with CD16/CD32 antibody (BD Pharmingen), cells were stained with fluorophore-conjugated antibodies: CD11b BV605 (1:200, clone M1/70, Biolegend) and CD11c APC (1:100, clone N418, Biolegend) on ice for 30-60 min. After washing, cells were incubated with dead cell dye, Zombie red (1:1000 in PBS, Biolegend) for 15 min on ice. Cells were fixed for 15 min on ice using BD Cytofix/Cytoperm reagent. After washing with BD Perm/Wash, cells were incubated overnight with phospho-p38 MAPK PE (Thr180/Tyr182 (3D7), 1:50, Cell Signaling). Cells were analyzed on Attune NxT Acoustic Focusing Cytometer (Life Technologies). Unstained cells, single stain controls, stained AbC Total Antibody Compensation beads and isotype controls were used for each experiment. Acquired data were analyzed using FlowJo software (TreeStar).

RNA isolation and qPCR

Transcription levels of CCL2 was examined in the lumbar spinal cords using qPCR as described earlier (25). Briefly, mice were anesthetized and transcardially perfused with ice cold PBS. Lumbar

spinal cords were dissected and stored separately in liquid nitrogen. Total RNA was isolated from spinal cord tissue using Direct-zol RNA MiniPrep Kit (Zymo Research) following the standard protocol. For analysis, RNA at purity $OD_{260/280}$ ratio between 1.8 and 2.0 was reverse-transcribed to cDNA using Multiscribe reverse transcriptase (Applied Biosystems). TaqMan gene expression assay (Applied Biosystems) was used for *CCL2* (Mm00441242_m1). All experimental samples were normalized to the expression level of *GAPDH* (4352339E Applied Biosystems). Relative quantification of fold-change was performed by applying the $2^{-\Delta\Delta}$CT method and comparing Cp values of individual mice (51).

Statistics

Statistical analysis was performed using GraphPad Prism 7.5. The numbers of animals per group used for each study are shown in the figures as individual dots or indicated in the figure legends. EAE clinical scores were pooled from four independent EAE experiments and evaluated for statistical significance using Two-way ANOVA with Sidak's multiple comparisons test. One-way ANOVA with Tukey's post hoc test was used to analyze EAE data shown in Table 1. Two group experiments were analyzed using Student's t-test. Experiments with three and more groups were analyzed using One-way ANOVA with Tukey's post hoc test. In all figures, data are represented as mean ± s.e.m. In all cases, probability values less than 0.05 were considered statistically significant. Images were assembled using Adobe Illustrator CC.

Author contributions

O.V.C. and F.M. designed research; O.V.C., F.M., Z.D., A.Z., D.J.D., and A.M.H. performed experiments; O.V.C., F.M., P.B., D.P., A.S., and W.D. interpreted the data, wrote and edited manuscript.

Acknowledgments

This work was in parts supported by grants from National Institutes of Health (R01HD087566 and R01HD091325 to W.D.) and Shriners Hospital for Children (87310 to O.C.).

References

1. Coret F, *et al.* (2018) Onset of secondary progressive multiple sclerosis is not influenced by current relapsing multiple sclerosis therapies. *Mult Scler J Exp Transl Clin* 4(2):2055217318783347.
2. Zhang T, *et al.* (2015) Beta-interferon exposure and onset of secondary progressive multiple sclerosis. *Eur J Neurol* 22(6):990-1000.
3. Ontaneda D, Fox RJ, & Chataway J (2015) Clinical trials in progressive multiple sclerosis: lessons learned and future perspectives. *Lancet Neurol* 14(2):208-223.
4. Scalfari A, Neuhaus A, Daumer M, Muraro PA, & Ebers GC (2014) Onset of secondary progressive phase and long-term evolution of multiple sclerosis. *J Neurol Neurosurg Psychiatry* 85(1):67-75.
5. Giles DA, Duncker PC, Wilkinson NM, Washnock-Schmid JM, & Segal BM (2018) CNS-resident classical DCs play a critical role in CNS autoimmune disease. *J Clin Invest* 128(12):5322-5334.
6. Mundt S, *et al.* (2019) Conventional DCs sample and present myelin antigens in the healthy CNS and allow parenchymal T cell entry to initiate neuroinflammation. *Sci Immunol* 4(31).
7. Greter M, *et al.* (2005) Dendritic cells permit immune invasion of the CNS in an animal model of multiple sclerosis. *Nat Med* 11(3):328-334.
8. King IL, Dickendesher TL, & Segal BM (2009) Circulating Ly-6C+ myeloid precursors migrate to the CNS and play a pathogenic role during autoimmune demyelinating disease. *Blood* 113(14):3190-3197.
9. Giles DA, *et al.* (2018) Myeloid cell plasticity in the evolution of central nervous system autoimmunity. *Ann Neurol* 83(1):131-141.
10. Kamphuis W, Kooijman L, Schetters S, Orre M, & Hol EM (2016) Transcriptional profiling of CD11c-positive microglia accumulating around amyloid plaques in a mouse model for Alzheimer's disease. *Biochim Biophys Acta* 1862(10):1847-1860.
11. Prodinger C, *et al.* (2011) CD11c-expressing cells reside in the juxtavascular parenchyma and extend processes into the glia limitans of the mouse nervous system. *Acta Neuropathol* 121(4):445-458.
12. Wlodarczyk A, *et al.* (2015) Pathologic and Protective Roles for Microglial Subsets and Bone Marrow- and Blood-Derived Myeloid Cells in Central Nervous System Inflammation. *Front Immunol* 6:463.
13. Ford AL, Goodsall AL, Hickey WF, & Sedgwick JD (1995) Normal adult ramified microglia separated from other central nervous system macrophages by flow cytometric sorting. Phenotypic differences defined and direct ex vivo antigen presentation to myelin basic protein-reactive CD4+ T cells compared. *J Immunol* 154(9):4309-4321.
14. Miller SD, McMahon EJ, Schreiner B, & Bailey SL (2007) Antigen presentation in the CNS by myeloid dendritic cells drives progression of relapsing experimental autoimmune encephalomyelitis. *Ann N Y Acad Sci* 1103:179-191.
15. Fischer HG & Reichmann G (2001) Brain dendritic cells and macrophages/microglia in central nervous system inflammation. *J Immunol* 166(4):2717-2726.
16. Serafini B, Columba-Cabezas S, Di Rosa F, & Aloisi F (2000) Intracerebral recruitment and maturation of dendritic cells in the onset and progression of experimental autoimmune encephalomyelitis. *Am J Pathol* 157(6):1991-2002.
17. Wlodarczyk A, *et al.* (2018) CSF1R Stimulation Promotes Increased Neuroprotection by CD11c+ Microglia in EAE. *Front Cell Neurosci* 12:523.
18. Sato-Hashimoto M, *et al.* (2019) Microglial SIRPalpha regulates the emergence of CD11c(+) microglia and demyelination damage in white matter. *Elife* 8.
19. Butovsky O, *et al.* (2006) Glatiramer acetate fights against Alzheimer's disease by inducing dendritic-like microglia expressing insulin-like growth factor 1. *Proceedings of the National Academy of Sciences of the United States of America* 103(31):11784-11789.
20. Zarubin T & Han J (2005) Activation and signaling of the p38 MAP kinase pathway. *Cell Res* 15(1):11-18.
21. Lock C, *et al.* (2002) Gene-microarray analysis of multiple sclerosis lesions yields new targets validated in autoimmune encephalomyelitis. *Nat Med* 8(5):500-508.
22. Huang G, *et al.* (2012) Signaling via the kinase p38alpha programs dendritic cells to drive TH17 differentiation and autoimmune inflammation. *Nat Immunol* 13(2):152-161.

23. Di Mitri D, *et al.* (2015) The p38 mitogen-activated protein kinase cascade modulates T helper type 17 differentiation and functionality in multiple sclerosis. *Immunology* 146(2):251-263.
24. Krementsov DN, *et al.* (2014) Sex-specific control of central nervous system autoimmunity by p38 mitogen-activated protein kinase signaling in myeloid cells. *Ann Neurol* 75(1):50-66.
25. Chechneva OV, *et al.* (2011) Low dose dextromethorphan attenuates moderate experimental autoimmune encephalomyelitis by inhibiting NOX2 and reducing peripheral immune cells infiltration in the spinal cord. *Neurobiol Dis* 44(1):63-72.
26. Babaloo Z, *et al.* (2015) The role of Th17 cells in patients with relapsing-remitting multiple sclerosis: interleukin-17A and interleukin-17F serum levels. *Immunol Lett* 164(2):76-80.
27. Balashov KE, Smith DR, Khoury SJ, Hafler DA, & Weiner HL (1997) Increased interleukin 12 production in progressive multiple sclerosis: induction by activated CD4+ T cells via CD40 ligand. *Proceedings of the National Academy of Sciences of the United States of America* 94(2):599-603.
28. Romme Christensen J, *et al.* (2013) Systemic inflammation in progressive multiple sclerosis involves follicular T-helper, Th17- and activated B-cells and correlates with progression. *PLoS One* 8(3):e57820.
29. Gold R, Linington C, & Lassmann H (2006) Understanding pathogenesis and therapy of multiple sclerosis via animal models: 70 years of merits and culprits in experimental autoimmune encephalomyelitis research. *Brain* 129(Pt 8):1953-1971.
30. Ajami B, Bennett JL, Krieger C, McNagny KM, & Rossi FM (2011) Infiltrating monocytes trigger EAE progression, but do not contribute to the resident microglia pool. *Nat Neurosci* 14(9):1142-1149.
31. Dogan RN, Elhofy A, & Karpus WJ (2008) Production of CCL2 by central nervous system cells regulates development of murine experimental autoimmune encephalomyelitis through the recruitment of TNF- and iNOS-expressing macrophages and myeloid dendritic cells. *J Immunol* 180(11):7376-7384.
32. Tran EH, Hoekstra K, van Rooijen N, Dijkstra CD, & Owens T (1998) Immune invasion of the central nervous system parenchyma and experimental allergic encephalomyelitis, but not leukocyte extravasation from blood, are prevented in macrophage-depleted mice. *J Immunol* 161(7):3767-3775.
33. Merad M, Sathe P, Helft J, Miller J, & Mortha A (2013) The dendritic cell lineage: ontogeny and function of dendritic cells and their subsets in the steady state and the inflamed setting. *Annu Rev Immunol* 31:563-604.
34. Adelmann M, *et al.* (1995) The N-terminal domain of the myelin oligodendrocyte glycoprotein (MOG) induces acute demyelinating experimental autoimmune encephalomyelitis in the Lewis rat. *J Neuroimmunol* 63(1):17-27.
35. Tanabe S, Saitoh S, Miyajima H, Itokazu T, & Yamashita T (2019) Microglia suppress the secondary progression of autoimmune encephalomyelitis. *Glia* 67(9):1694-1704.
36. Encinas JA, *et al.* (1999) QTL influencing autoimmune diabetes and encephalomyelitis map to a 0.15-cM region containing Il2. *Nat Genet* 21(2):158-160.
37. Basso AS, *et al.* (2008) Reversal of axonal loss and disability in a mouse model of progressive multiple sclerosis. *J Clin Invest* 118(4):1532-1543.
38. Mathews CE, *et al.* (2015) Acute Versus Progressive Onset of Diabetes in NOD Mice: Potential Implications for Therapeutic Interventions in Type 1 Diabetes. *Diabetes* 64(11):3885-3890.
39. Moreno M, *et al.* (2014) Conditional ablation of astroglial CCL2 suppresses CNS accumulation of M1 macrophages and preserves axons in mice with MOG peptide EAE. *J Neurosci* 34(24):8175-8185.
40. Taves S, *et al.* (2016) Spinal inhibition of p38 MAP kinase reduces inflammatory and neuropathic pain in male but not female mice: Sex-dependent microglial signaling in the spinal cord. *Brain, behavior, and immunity* 55:70-81.
41. Sorge RE, *et al.* (2015) Different immune cells mediate mechanical pain hypersensitivity in male and female mice. *Nat Neurosci* 18(8):1081-1083.
42. Angele MK, *et al.* (2003) Sex-specific p38 MAP kinase activation following trauma-hemorrhage: involvement of testosterone and estradiol. *Am J Physiol Endocrinol Metab* 285(1):E189-196.
43. Krementsov DN, Thornton TM, Teuscher C, & Rincon M (2013) The emerging role of p38 mitogen-activated protein kinase in multiple sclerosis and its models. *Mol Cell Biol* 33(19):3728-3734.
44. Goldstein DM, Kuglstatter A, Lou Y, & Soth MJ (2010) Selective p38alpha inhibitors clinically evaluated for the treatment of chronic inflammatory disorders. *J Med Chem* 53(6):2345-2353.

45. Owens T, Bechmann I, & Engelhardt B (2008) Perivascular spaces and the two steps to neuroinflammation. *J Neuropathol Exp Neurol* 67(12):1113-1121.
46. Berger T*, et al.* (1997) Experimental autoimmune encephalomyelitis: the antigen specificity of T lymphocytes determines the topography of lesions in the central and peripheral nervous system. *Lab Invest* 76(3):355-364.
47. Sedgwick J, Brostoff S, & Mason D (1987) Experimental allergic encephalomyelitis in the absence of a classical delayed-type hypersensitivity reaction. Severe paralytic disease correlates with the presence of interleukin 2 receptor-positive cells infiltrating the central nervous system. *J Exp Med* 165(4):1058-1075.
48. McRae BL, Vanderlugt CL, Dal Canto MC, & Miller SD (1995) Functional evidence for epitope spreading in the relapsing pathology of experimental autoimmune encephalomyelitis. *J Exp Med* 182(1):75-85.
49. Lo U*, et al.* (2014) p38alpha (MAPK14) critically regulates the immunological response and the production of specific cytokines and chemokines in astrocytes. *Sci Rep* 4:7405.
50. Shi LZ*, et al.* (2011) HIF1alpha-dependent glycolytic pathway orchestrates a metabolic checkpoint for the differentiation of TH17 and Treg cells. *J Exp Med* 208(7):1367-1376.
51. Livak KJ & Schmittgen TD (2001) Analysis of relative gene expression data using real-time quantitative PCR and the 2(-Delta Delta C(T)) Method. *Methods* 25(4):402-408.

Figures and figure legends

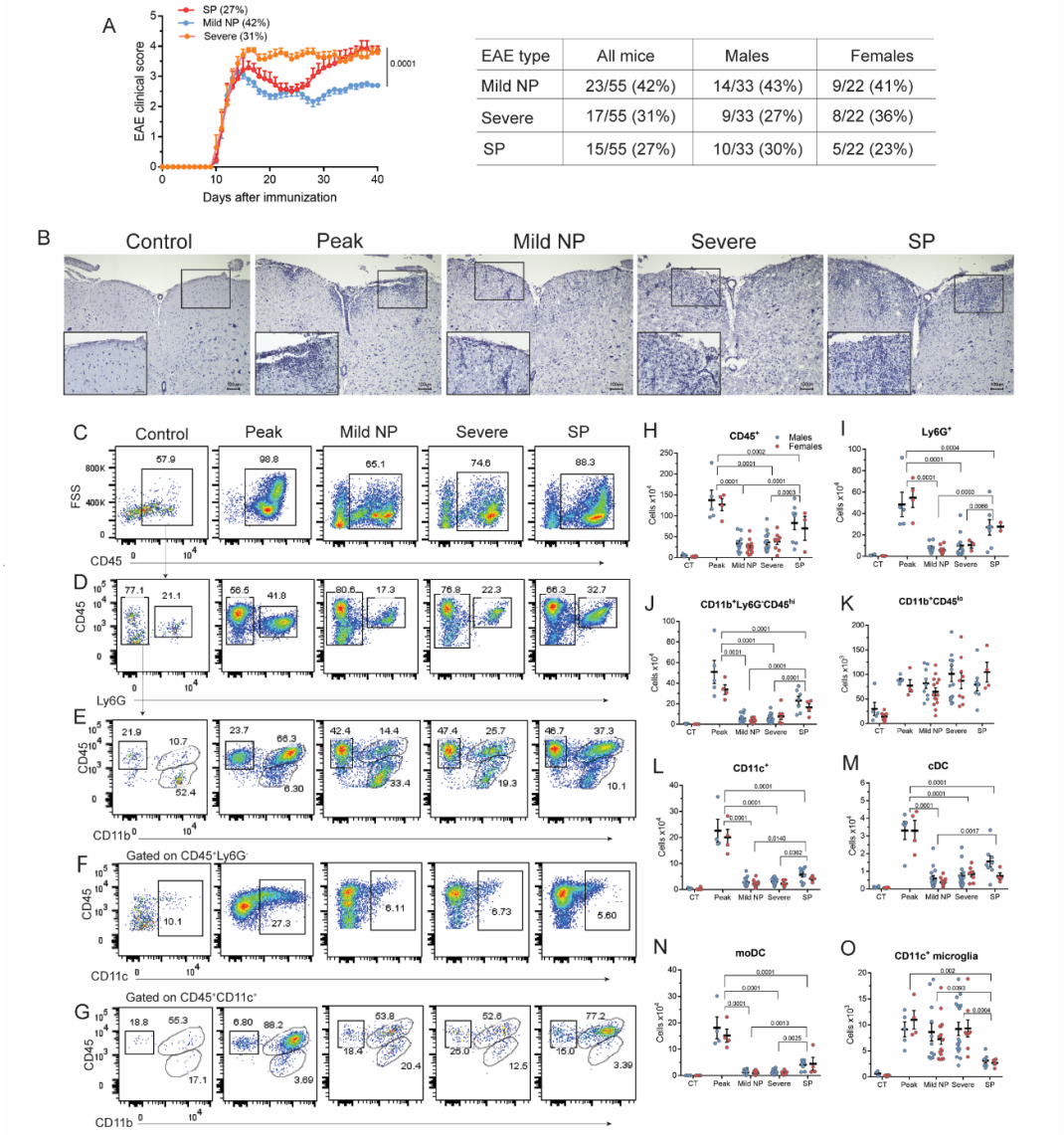

EAE type	All mice	Males	Females
Mild NP	23/55 (42%)	14/33 (43%)	9/22 (41%)
Severe	17/55 (31%)	9/33 (27%)	8/22 (36%)
SP	15/55 (27%)	10/33 (30%)	5/22 (23%)

Fig. 1. Reduction in CD11c$^+$ microglia and diffuse parenchymal infiltration are distinct in EAE SP in WT mice.

(A) EAE was induced in C57BL/6 mice with MOG$_{35-55}$ prepared by syringe homogenization. Animals were grouped based on clinical phenotype around 30 days of EAE: mild non-progressive (NP), severe or secondary progressive (SP). (B) H&E staining of lumbar spinal cord in healthy control, at EAE peak (13-16 dpi), and in chronic mild NP, severe and SP EAE. Scale bar 100 µm. Cells were isolated from the brain and spinal cord of healthy mice, at EAE peak, mild NP, severe and SP EAE mice and analyzed by flow cytometry. FACS analysis of CD45$^+$ cells (C), Ly6G$^+$ neutrophils (D), CD11b$^+$CD45^{hi}Ly6G$^-$ macrophages/monocytes and CD11b$^+$CD45^{lo} microglia (E), CD11c$^+$ cells (F). Gating strategy to differentiate cDC, moDC and CD11c$^+$ microglia by expression of CD45 and CD11b (G). Quantification of CD45$^+$ cells (H), Ly6G$^+$ neutrophils (I), macrophages/monocytes (J), microglia (K), CD11c$^+$ cells (L), cDC (M), moDC (N) and CD11c$^+$ microglia (O). Data are representative of six independent experiments. Each point represents an individual animal. *P* values were determined by One-way ANOVA with Tukey's post hoc test.

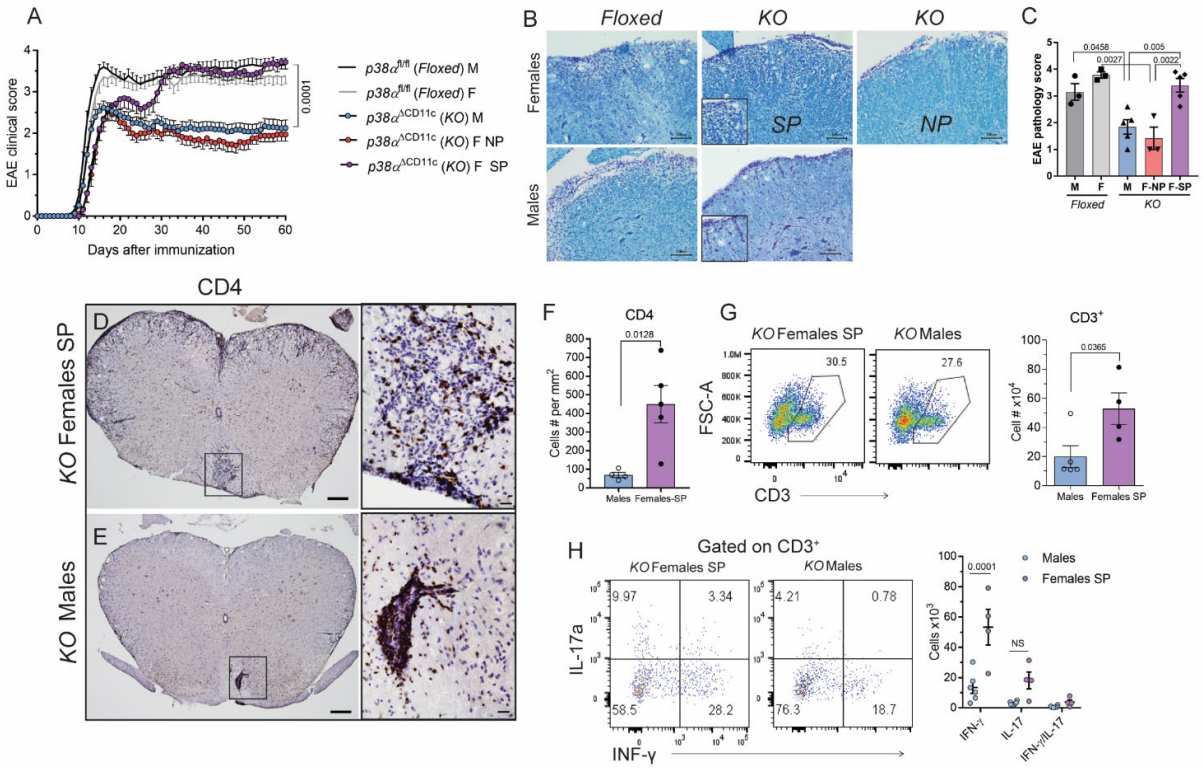

Fig. 2. Knockout of *p38α* in CD11c$^+$ cells triggers SP EAE in females.
p38α$^{fl/fl}$ (*Floxed*) and p38α$^{\Delta CD11c}$ (*KO*) female and male mice were immunized with MOG-PTX to induce EAE. (A) EAE clinical scores were monitored daily through day 60 post immunization. Data are representative of four independent experiments with n = 47 for *KO* males, n = 23 for *KO* females with secondary progression (SP), n = 17 for *KO* females without secondary progression (NP), n = 41 for *Floxed* males and n = 32 for *Floxed* females. *P* values were determined by two-way ANOVA with Sidak's multiple comparisons test; (B) Representative image of LFB staining of the lumbar spinal cord of *Floxed* and *KO* male and female mice around day 30 post EAE induction. Note two pathological phenotypes in *KO* female mice. Scale bar 100 µm. (C) EAE pathological score based on the degree of infiltration and demyelination. Data are representative of two independent experiments. *P* values were determined by One-way ANOVA with Tukey's post hoc test. CD4$^+$ T cells in the lumbar spinal cord of *KO* SP female (D) and *KO* male (E) mice. CD4$^+$ cell distribution in the dorsal lumbar spinal cord (D-E, enlargements). Scale bars 200 µm for D-E, 20 µm for enlargements. (F) Quantitative analysis of CD4$^+$ cells in white matter parenchyma of lumbar spinal cord. (G) CD3$^+$ T cells detected by flow cytometry in the brain and spinal cord of *KO* male and *KO* SP female mice. (H) FACS analysis of IL-17a$^+$ and IFN-γ$^+$ T cells isolated from the CNS of *KO* male and *KO* SP female mice. Data are representative of two independent experiments. *P* values were determined by Student's t-test. Each circle represents an individual mouse and small horizontal line indicates the mean. NS, not significant.

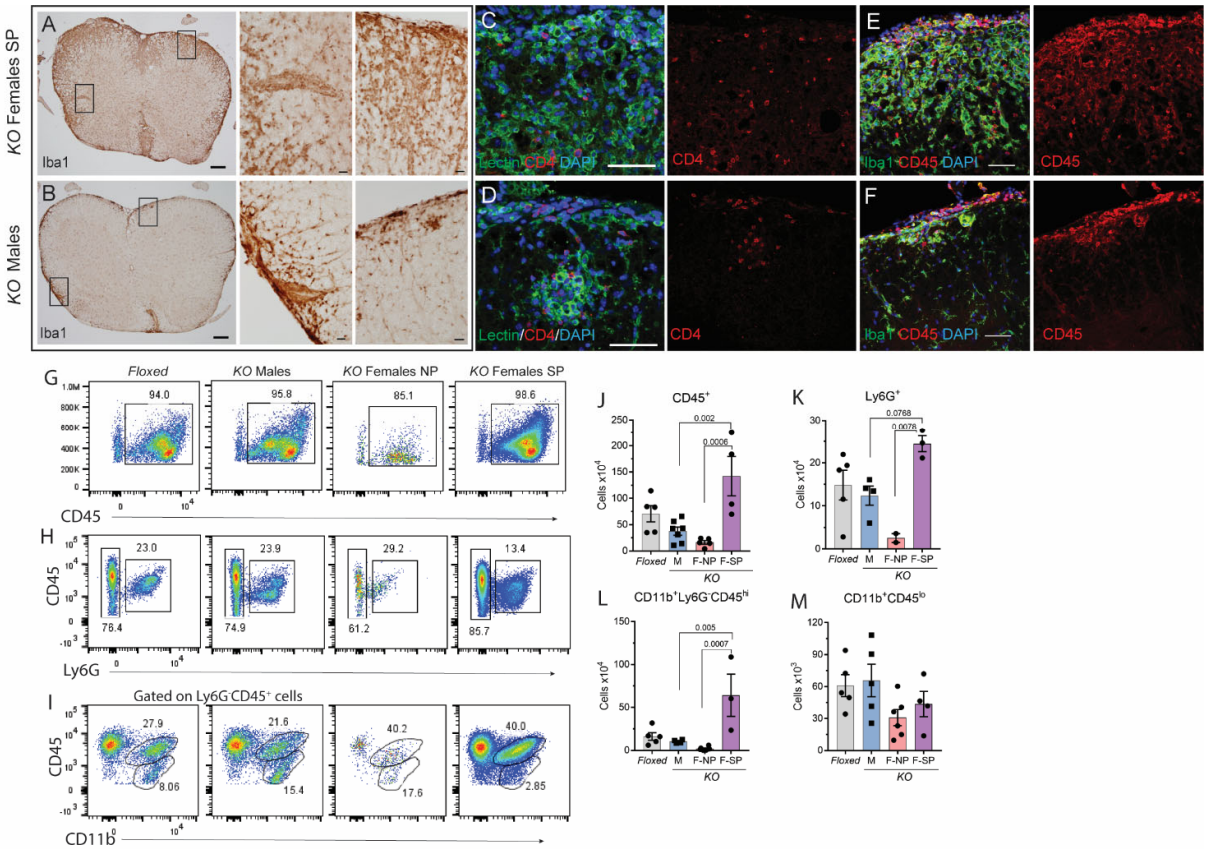

Fig. 3. Knockout of p38α in CD11c$^+$ cells permits myeloid cell CNS invasion in females. Iba1$^+$ cells in the lumbar spinal cord of *KO* SP female (A) and *KO* male (B) mice around 30 dpi. Iba1$^+$ cells in the lateral and ventral lumbar spinal cord (A-B, enlargements). Infiltrating lectin$^+$ macrophages/monocytes and CD4$^+$ T cells in the ventral lumbar spinal cord of *KO* SP female (C) and *KO* male (D) mice. Pattern of CD45$^+$ cell infiltration in *KO* SP female (E) and *KO* male (F) mice. Scale bars 200 µm for A-B, 20 µm for enlargements in A-B; 50 µm for C-F. FACS analysis of CD45$^+$ cells (G), neutrophils (H), macrophages/monocytes and microglia (I) isolated from the brain and spinal cord of *KO* male and *KO* SP female mice. Quantification of isolated CD45$^+$ cells (J), Ly6G$^+$ neutrophils (K), macrophages/monocytes (L) and microglia (M). Data are representative of three independent experiments. Each point represents an individual animal. P values were determined by One-way ANOVA with Tukey's post hoc test. M, males; F, females; F-SP, secondary progressed females, F-NP, non-progressed females.

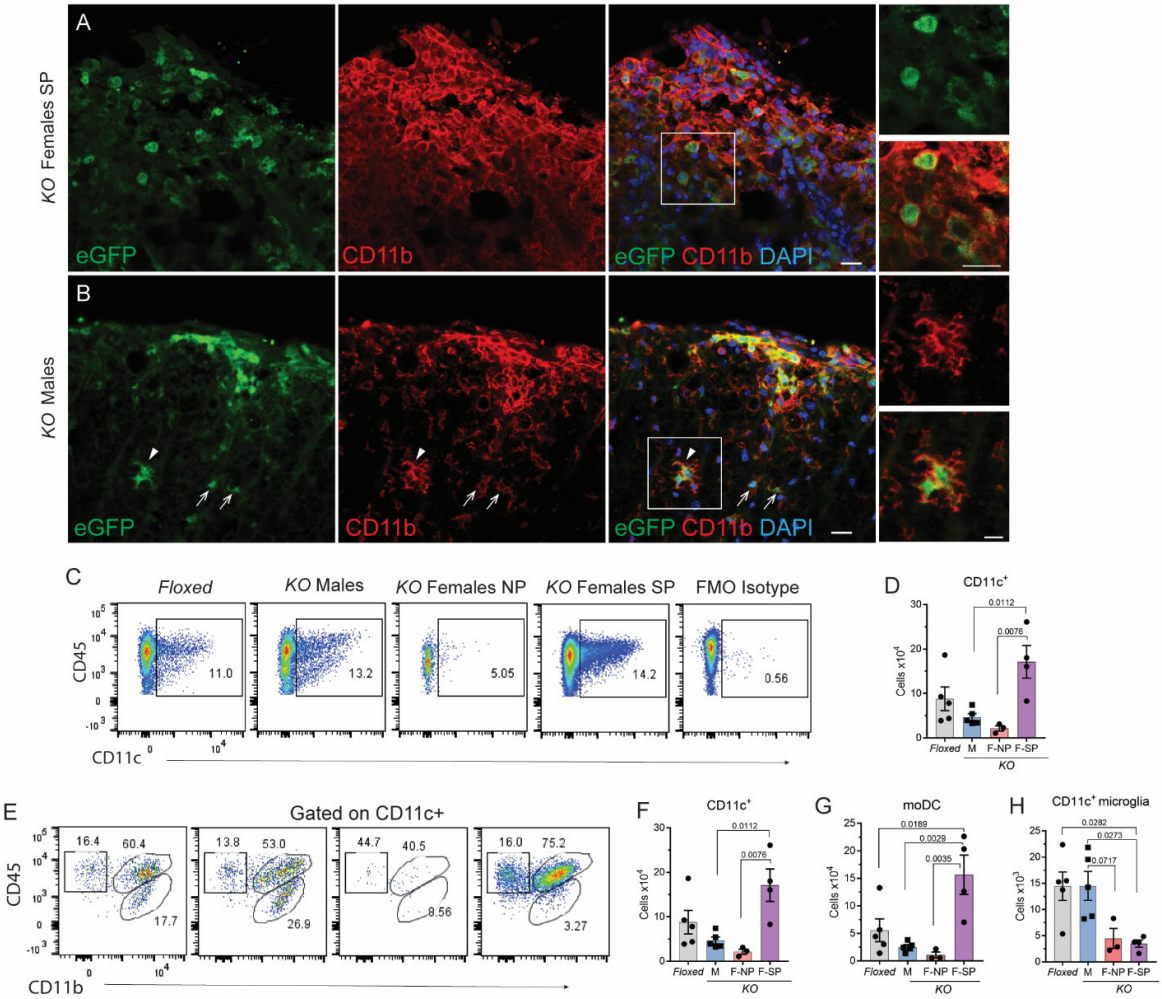

Fig. 4. CD11c$^+$ microglia are reduced in females lacking *p38α* in CD11c$^+$ cells.
CD11c$^+$ cells were detected using *CD11c*-promoter driven expression of eGFP. (A) eGFP$^+$CD11b$^+$ cells with macrophage/reactive microglia morphology in the lumbar spinal cord parenchyma of *KO* SP females. (B) In males, eGFP$^+$ cells co-expressing CD11b were found at the meninges. eGFP$^+$ microglia (arrows) and microglia with dendritic cell morphology (arrowhead and enlargement) in white matter of the ventral lumbar spinal cord in *KO* males. Scale bars 20 µm for A, B; 25 µm for enlargement in A; 10 µm for enlargement in B. (C) Flow cytometry analysis of CD11c$^+$ cells isolated from the brain and spinal cord of *Floxed* mice, *KO* males and *KO* females with secondary progression (SP) and without (NP) around day 30 dpi. (D) Quantification of CD11c$^+$ cells determined by FACS. (E) CD11c$^+$ cells gating on CD45 and CD11b. Quantification of CD11c$^+$CD11b$^-$CD45^{hi} cDC (F), CD11c$^+$CD11b$^+$CD45^{hi} moDC (G) and CD11c$^+$CD11b$^+$CD45^{lo} microglia (H). Data are representative of three independent experiments. Each point represents an individual animal. *P* values were determined by One-way ANOVA with Tukey's post hoc test. M, males; F-SP, secondary progressed females, F-NP, non-progressed females.

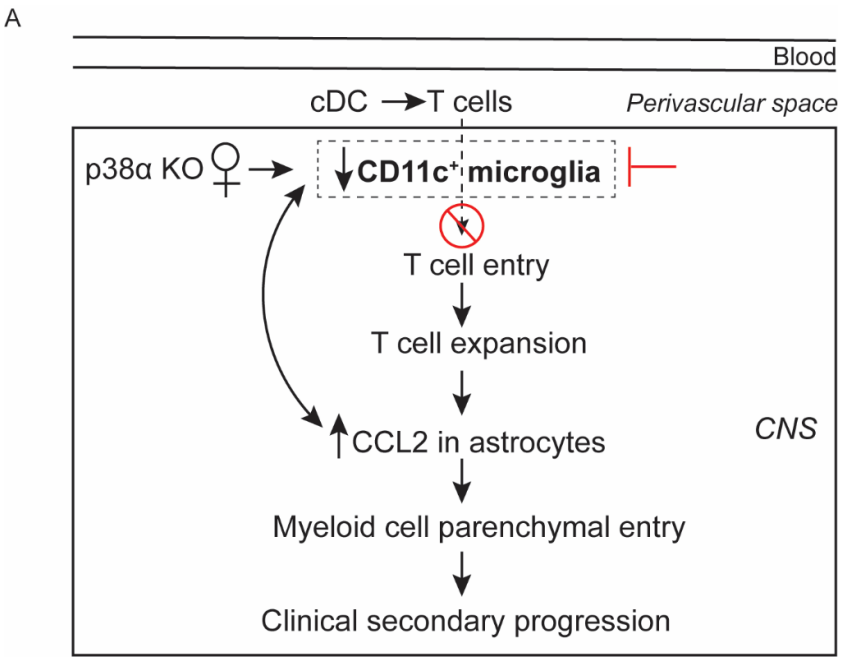

Fig. 5. Cellular interaction model of SP EAE.
T cells are reactivated by cDC in the leptomeninges and perivascular spaces separated from CNS parenchyma by the basement membrane and glia limitans. Reduction in $CD11c^+$ microglia allows T cells to cross the basement membrane and glia limitans and enter CNS parenchyma. T cells expand within CNS parenchyma, causing clinical onset of EAE SP. Increase in astrocyte derived CCL2 induces myeloid cell parenchymal infiltration. Invading myeloid cells injure oligodendrocytes, myelin and axons, causing exacerbation of EAE clinical symptoms and SP.

Tables

Table 1. EAE clinical characteristics in *p38α*$^{fl/fl}$ (*Floxed*) and *p38α*$^{\Delta CD11c}$ (*KO*) female and male mice

Group	n	Onset	Mean score 1st peak	Mean score d26	Mean score d32	Max severity from d29	Duration of paralysis d29 – d60	Score at d60	Survival
Floxed males	41	11.2 ± 0.2	4.2 ± 0.1	3.2 ± 0.2	3.4 ± 0.2	3.9 ± 0.1	25.9 ± 1.8	3.7 ± 0.2	90.2%
Floxed females	32	12.4 ± 0.4	4.0 ± 0.1	3.2 ± 0.2	3.3 ± 0.2	3.7 ± 0.2	23.9 ± 2.3	3.4 ± 0.2	90.6%
KO males	47	12.2 ± 0.3	3.3 ± 0.1***	2.2 ± 0.2***	2.1 ± 0.2***	2.7 ± 0.2***	10.0 ± 2.1***	2.1 ± 0.2***	95.7%
KO females NP	17	13.2 ± 0.4*	2.9 ± 0.2***	2.0 ± 0.2***	2.1 ± 0.1**	2.3 ± 0.1***	0 ***	2.0 ± 0.2***	100%
KO females SP	23	14.6 ± 0.8$^{\#\#\#}$	3.6 ± 0.2$^{\$}$	2.6 ± 0.3	3.5 ± 0.2$^{\#\#\#}$	4.1 ± 0.1$^{\#\#\#}$	19.4 ± 2.5$^{\#}$	3.7 ± 0.2$^{\#\#\#}$	91.3%

Data are the mean ± s.e.m. **P*<0.05, ***P*<0.01, ****P*<0.001, comparing between same sex *Floxed* and *KO* mice. $^{\#}$*P*<0.05, $^{\#\#\#}$*P*<0.01, comparing between females and males of the same genotype. $^{\$}$*P*<0.05, comparing between KO females with and without secondary progression (SP and NP). *P* values were determined by One-way ANOVA with Tukey's post hoc test.